

LOG-LIO: A LiDAR-Inertial Odometry with Efficient Local Geometric Information Estimation

Kai Huang¹, Junqiao Zhao^{*,2,3}, Tiantian Feng¹, Zhongyang Zhu³, Chen Ye²

Abstract—Local geometric information, i.e. normal and point distribution, is crucial for LiDAR-based simultaneous localization and mapping (SLAM) because it provides constraints for data association, which further determines the direction of optimization and ultimately affects the accuracy of poses. However, estimating normal and point distribution are time-consuming tasks even with the assistance of the KDtree or volumetric maps. To achieve fast normal estimation, we look into the structural information of LiDAR scan and propose a novel fast approximate least squares (FALS) method. With the pre-computed bearing information, estimating the normal requires only the range information of the points when a new scan arrives. To efficiently estimate the distribution of points, we extend the ikd-tree to manage the map in voxels and update its point cloud distribution incrementally while maintaining its consistency with the normals. For scan points that satisfy visibility and consistency checks based on normal, we devise a robust and accurate hierarchical data association schema considering the distribution where point-to-surfel is prioritized over point-to-plane. We further fix voxels after the distribution convergences to balance the time consumption and the correctness of representation. Extensive experiments on diverse public datasets demonstrate the advantages of our system compared to other state-of-the-art methods.

I. INTRODUCTION

Simultaneous localization and mapping (SLAM) plays an important role in autonomous driving and robotics tasks. LiDAR(-inertial) systems [1]–[4] are robust and accurate because they are less sensitive to illumination changes and have a larger field of view (FoV).

The accuracy of LiDAR-based system depends on the registration between point cloud and map, which associates them according to the similarity of local geometric information and then minimizes their distances. Therefore, accurate and fast estimation of local geometric information has gained increasing attention in recent studies [4]–[8]. Normal and point distribution are two representative local geometric properties of the surface where a point is located, but estimating any one of them is a time-consuming task for LiDAR-

inertial odometry (LIO) systems even with the assistance of the KDtree or volumetric maps. Therefore the previous LIO systems seldom incorporate the real-time estimation of normal and point distribution, which may undermine the real-time performance of the systems.

The conventional method for estimating local geometric information is to evaluate the smoothness of the input scan points and fit the features to the map points, respectively [9]. Further, optimization minimizes the distance from the point to the corresponding feature along the normal direction, which also depends on the local geometric information. However, simple smoothness calculations do not take into account information about adjacent scan lines, and the coordinates of map points do not accurately represent the spatial distribution of neighbors, which may degrade the accuracy of the LIO system. Estimating local geometric information efficiently in the LIO system remains a challenge.

This paper presents LOG-LIO, a robust and accurate LIO system focusing on the estimation of local geometric information, including efficiently estimating the normal of LiDAR scanning points and the distribution of map points, and their rational utilization.

Inspired by [10] and [11], we look into the structural information of LiDAR scan and propose a novel fast approximate least squares (FALS) method. We project point cloud onto the range image to pre-build a lookup table, which stores the bearing information for the certain LiDAR. With the arrival of a new scan, only the range of the point is needed to estimate the normal, and the matrix inversion operation is not performed in the calculation, which greatly improves the efficiency.

We incrementally update the point cloud distribution within the map voxels to keep the correctness of the spatial information while maintaining its consistency with the normals. To balance time consumption and correctness of representation, we manage the map on the extended ikd-tree and further fix the distribution after it converges.

The main contributions of this work are listed as follows:

- Ring FALS, a novel fast approximate least squares normal estimator using the structural information of certain LiDAR, is fast and accurate compared to PCL, and meets the real-time requirements of the LIO system.
- A robust and accurate hierarchical data association schema considering the distribution of points within map voxels where point-to-surfel is prioritized over point-to-plane and large-scale over small-scale.
- Extensive experiments on public datasets demonstrate the advantages of our LIO system compared to other

¹Kai Huang and Tiantian Feng are with the School of Surveying and Geo-Informatics, Tongji University, Shanghai, China (e-mail: huangkai@tongji.edu.cn; fengtiantian@tongji.edu.cn).

This work is supported by the National Key Research and Development Program of China (No. 2021YFB2501104). (Corresponding Author: Junqiao Zhao.)

²Junqiao Zhao, Zhongyang Zhu and Chen Ye are with Department of Computer Science and Technology, School of Electronics and Information Engineering, Tongji University, Shanghai, China, and the MOE Key Lab of Embedded System and Service Computing, Tongji University, Shanghai, China (Corresponding Author: zhaojunqiao@tongji.edu.cn; 1930773@tongji.edu.cn; yechen@tongji.edu.cn).

³Institute of Intelligent Vehicles, Tongji University, Shanghai, China

state-of-the-art methods. To benefit the community, our implementation of this work is open-source at <https://github.com/tiev-tongji/LOG-LIO>, and we also open-source Ring FALS as an independent normal tool at <https://github.com/tiev-tongji/RingFalsNormal>.

II. RELATED WORKS

A. Point Cloud Normal Estimation

The most common method to obtain surface normals from point cloud is the least squares due to its relatively low computational cost and ease of implementation [12]. However, even without considering the disorderly nature of LiDAR point cloud, the least squares method is computationally expensive for LIO systems. [10] compares the complexity of least squares approaches, and by reformulating the traditional least squares solution, the normal can be estimated by calculating the derivatives of surface from a spherical range image (SRI). However, with a large k neighborhood, usually k greater than 5 is more reliable, the time consumption of SRI is greater than FALS. 3F2N [11] simply performs three filtering operations on the inverse depth image to estimate the normals, which is slightly faster than FALS, and the accuracy is strongly influenced by the filter. However, 3F2N is designed for RGBD camera point cloud and requires neighborhood information of pixels, making it not directly applicable to LiDAR point cloud.

Inspired by [10] and [11], we propose Ring FALS, a normal estimator for LiDAR point cloud. By analyzing the spatial geometric information of the disordered LiDAR point cloud, we pre-compute and store its structural information in a lookup table.

B. Points Distribution Estimation

LOAM [9] does not estimate the distribution of points, but performs eigen analysis on the associated map points to determine whether its local geometry is close to a line or a plane. However, the coordinates of a few neighborhood points cannot accurately represent local geometric information, which results in providing inaccurate constraints.

Different from the LOAM point-to-line and point-to-plane ICP algorithm, DLO [5] registers point cloud using Generalized ICP (GICP) [13] to minimize the plane-to-plane distances, and these planes are modeled by the computed covariance of each point in the scan. It assumes that the submap covariances can be approximated by concatenating the normals from keyframes and the covariance of the points is only computed once when the scan is acquired. However, such a stitching normals method cannot accurately represent the local geometric information of the point cloud, which ultimately affects accuracy.

LOCUS 2.0 [4] extends the work of LOCUS [7], which constructs custom covariance matrices based on the pre-computed normals for GICP, but how to pre-compute normals is not elaborated in their paper.

Wildcat [8] generate surfels by clustering points based on their coordinates and timestamps, and then fits ellipsoids to them based on the distribution of point coordinates. Similar

to Wildcat, SLICT [6] proposes an octree-based global map and incrementally updates the point distribution within voxels incrementally. It obtains large-scale distribution by merging multiple voxels. Inspired by the above, we extend ikd-tree to maintain the positions and update points distribution of map nodes incrementally. We manage map nodes in the extended ikd-tree with voxels, and then fix the voxel to surfel after its distribution convergences.

C. LiDAR(-Inertial) Odometry

LOAM [9] has inspired many LiDAR SLAM systems due to the relative independence of the system modules and the rationality of using point cloud geometry attributes. However, the lack of effective map management and the huge optimization time consumption can reduce the performance of the system.

LIO-SAM proposes a framework based on keyframes and local maps, which optimizes poses in a factor graph [14]. However, LIO-SAM builds sub-maps for input scans by simply merging point cloud of surrounding keyframes, which is a time-consuming construction when the number of points is large. FAST-LIO [15] adopts the error-state iterated extended Kalman filter (iEKF) to directly register the undistorted point cloud and map. It presents a new formula to compute the Kalman gain and the computation load depends on the state dimension. FAST-LIO2 [16] maintains the map by an incremental KDtree data structure, namely ikd-tree, to further improve efficiency. In this paper, we adopt the iEKF as FAST-LIO to optimize poses by directly registering point cloud and map, but with a different data association schemas. By incorporating normal and points distribution, we construct surfel and associate with it in priority, since surfel is more representative of the local geometric properties of a small region.

III. PRELIMINARY

A. Notation

We now define notions and frame definitions that we used throughout the paper. We consider \mathcal{W} as the world frame and $\mathcal{I}_k, \mathcal{L}_k$ as the IMU and LiDAR frames, related to the k -th LiDAR scan at time t_k , respectively. ${}^a\mathbf{T}_b \in SE(3)$ to be Euclidean transformation take 3D points from frame b to frame a , which consisted of rotation ${}^a\mathbf{R}_b \in SO(3)$ and translation ${}^a\mathbf{t}_b \in \mathbb{R}^3$.

B. LiDAR Observation Model

In practice, LiDAR obtains the 3D coordinates of a point by combining bearing and range measurements of the target surface [17], [18], as shown in Fig. 1(a). The LiDAR observation model is as follows:

$$\mathbf{p}_i = r_i \mathbf{v}_i = r_i \begin{bmatrix} \cos \theta_i \cos \varphi_i \\ \sin \theta_i \cos \varphi_i \\ \sin \varphi_i \end{bmatrix} \quad (1)$$

where r_i is the range, θ_i the azimuth and φ_i the vertical angle of the target point. \mathbf{v} represents the horizontal and vertical

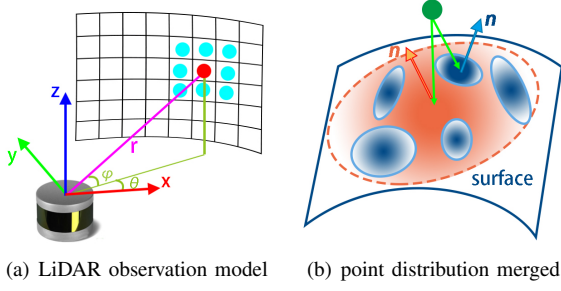


Fig. 1. Illustration of the LiDAR observation model and point distribution merged. (a) The magenta line indicates the range of the red point. The 8 cyan points are the neighborhoods that Ring FALS uses to estimate the normal of the target point. (b) The 5 blue ellipses represent the nearest neighbors of the green query point in the extended ikd-tree, and are merged into the large-scale orange distribution.

structural information of the point relative to the LiDAR. The inverse transformation is as follows:

$$\begin{bmatrix} r_i \\ \theta_i \\ \varphi_i \end{bmatrix} = \begin{bmatrix} \sqrt{x_i^2 + y_i^2 + z_i^2} \\ \arctan(y_i/x_i) \\ \arcsin(z_i/r_i) \end{bmatrix} \quad (2)$$

C. Least Squares Normal Estimation

Given a subset of n 3D points p_i , $i = 1, 2, \dots, n$ of the surface, least squares finds the normal vector $\mathbf{n} = (n_x, n_y, n_z)$ and the scalar d that minimizes

$$e = \sum_{i=1}^n (\mathbf{p}_i^T \mathbf{n} - d)^2 \quad (3)$$

The closed form solution of the normal \mathbf{n} is the eigenvector corresponding to the smallest eigenvalue of the covariance matrix

$$\mathbf{M} = \sum_{i=1}^n (\mathbf{p}_i - \bar{\mathbf{p}})(\mathbf{p}_i - \bar{\mathbf{p}})^T \quad (4)$$

with $\bar{\mathbf{p}} = 1/n \sum_{i=1}^n \mathbf{p}_i$.

D. Surfel

Similar to SLICT, the other quantities within the voxel can be calculated through the covariance matrix \mathbf{M} , as follows:

$$\begin{aligned} \rho_i &= 2 \frac{\lambda_2 - \lambda_1}{\lambda_1 + \lambda_2 + \lambda_3} \\ \gamma_i &= \lambda_2 / \lambda_1 \end{aligned} \quad (5)$$

where $\lambda_1, \lambda_2, \lambda_3$ are the eigenvalues of the covariance matrix \mathbf{M} with $\lambda_1 < \lambda_2 < \lambda_3$ and ρ_i represents planarity. A distribution satisfies surfel by having ρ_i greater than 1.0 and γ_i greater than 100, where a large ρ_i makes the distribution flatter and a large γ_i makes it less linear. A surfel represents a voxel with its mean position \mathcal{P}/n and \mathbf{n}_d , where \mathbf{n}_d is the eigenvector corresponding to λ_1 .

IV. SYSTEM OVERVIEW

The pipeline of LOG-LIO receives inputs from a 3D LiDAR and an IMU, as shown in Fig. 2. For a new input scan, we first use Ring FALS to estimate the normal of the raw points. After correcting distortion with IMU measurements, association is performed between the undistorted point cloud and the map according to their local geometric information. We integrate the measurements of IMU and optimize the poses of the body via iEKF, like FAST-LIO. After optimization, new points are added to the map managed by the extended ikd-tree, and the distribution within the voxel is incrementally maintained to ensure its accuracy while considering the normals, and fixed after convergence.

Our system takes IMU frame as the body frame, where system state \mathbf{x} can be written as:

$$\mathbf{x} = [\mathcal{W} \mathbf{R}_{\mathcal{I}}^T \quad \mathcal{W} \mathbf{p}_{\mathcal{I}}^T \quad \mathcal{W} \mathbf{v}_{\mathcal{I}}^T \quad \mathbf{b}_{\omega}^T \quad \mathbf{b}_a^T \quad \mathcal{W} \mathbf{g}^T] \quad (6)$$

where $\mathcal{W} \mathbf{R}_{\mathcal{I}}^T$, $\mathcal{W} \mathbf{p}_{\mathcal{I}}^T$ and $\mathcal{W} \mathbf{v}_{\mathcal{I}}^T$ are the attitude, position and velocity of IMU in the world frame (i.e., the first IMU frame), \mathbf{b}_{ω}^T and \mathbf{b}_a^T are gyroscope and accelerometer bias respectively, $\mathcal{W} \mathbf{g}^T$ is the known gravity vector in the world frame.

V. RING FALS NORMAL ESTIMATOR

For a LiDAR-based SLAM system, searching the neighborhood with the assistance of the KDtree and performing eigen analysis on the matrix \mathbf{M} in (4) are far overloaded.

In this paragraph, we revisit FALS [10]. Removing the scale factor d to eliminate the constraint on normal gives:

$$\tilde{e} = \sum_{i=1}^n (\mathbf{p}_i^T \tilde{\mathbf{n}} - 1)^2 \quad (7)$$

where $\tilde{\mathbf{n}}$ is defined up to a scale factor. By reformulating (7), the following is obtained:

$$\tilde{e} = \sum_{i=1}^n r_i^2 (\mathbf{v}_i^T \tilde{\mathbf{n}} - r_i^{-1})^2 \quad (8)$$

where r_i is the range and \mathbf{v}_i implies the bearing information of the target points related to LiDAR. Thanks to the high-resolution LiDAR, it can be assumed that the range of points within a small region are similar. Removing r_i^2 from (8) to obtain an approximation:

$$\hat{e} = \sum_{i=1}^n (\mathbf{v}_i^T \hat{\mathbf{n}} - r_i^{-1})^2 \quad (9)$$

the normal $\hat{\mathbf{n}}$ with the closed form solution $\hat{\mathbf{n}} = \widehat{\mathbf{M}}^{-1} \hat{\mathbf{b}}$ where $\widehat{\mathbf{M}} = \sum_{i=1}^n \mathbf{v}_i \mathbf{v}_i^T$ and $\hat{\mathbf{b}} = \sum_{i=1}^n \mathbf{v}_i / r_i$. The box-filtering techniques [19] are available to minimize the number of operations to compute the vector $\hat{\mathbf{b}}$ and the matrix $\widehat{\mathbf{M}}^{-1}$. Furthermore, the matrix $\widehat{\mathbf{M}}^{-1}$ depends only on the constant structural information \mathbf{v} , independent of the range r . Hence, the matrix $\widehat{\mathbf{M}}^{-1}$ can be precomputed as a lookup table for the certain LiDAR.

Obviously, a low-resolution lookup table can further improve the computational efficiency, which is similar to down-sampling. But in this work, we employ the Ring FALS to all

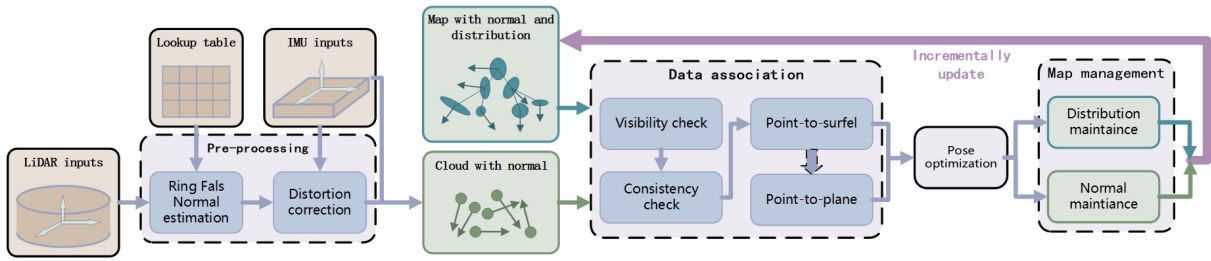


Fig. 2. System overview of LOG-LIO

new scan points for obtaining dense normals. Flipping the normals toward LiDAR and then applying image blurring techniques to smooth the normals can further improve the consistency of the local geometric information.

Notably, in the association module of LOAM, a point finds its k nearest points by traversing adjacent scanning lines, but this is still a time-consuming step. By pre-computing the lookup table, normal estimation avoids the slow searching process.

VI. POINTS DISTRIBUTION ESTIMATION

The widely used maps in SLAM systems record only the coordinates of points, and the sparsity of map points results in inaccurate representation of the environment, which may provide incorrect constraints and ultimately reduce the accuracy of pose estimation. To build a high-quality map, we incrementally maintain the points distribution within each voxel.

The distribution of points within a voxel can be represented by the covariance matrix \mathbf{M} in (4), which can be simplified as:

$$\mathbf{M} = \mathcal{S}_n - \frac{1}{n} \mathcal{P}_n \mathcal{P}_n^T \quad (10)$$

where \mathcal{S}_n denotes $\sum_{i=1}^n \mathbf{p}_i \mathbf{p}_i^T$ and \mathcal{P}_n denotes $\sum_{i=1}^n \mathbf{p}_i$. Due to the symmetric nature of the matrix \mathbf{M} , only the six elements in its upper right corner need to be recorded in the computation. Two distributions with n and m points, respectively, are merged as follows:

$$\mathbf{M}' = \mathcal{S}_n + \mathcal{S}_m - \frac{1}{n+m} (\mathcal{P}_n + \mathcal{P}_m) (\mathcal{P}_n + \mathcal{P}_m)^T \quad (11)$$

For a single point is added to the voxel that already has n points, one can use (11) and set m to 1.

The accurate representation of a distribution requires a large number of points. For a newly created voxel, only its \mathcal{S} , \mathcal{P} and the number of points need to be updated incrementally. Because of the limited FoV, for a high-quality map, point cloud should be collected from multiple places, which is historical and accumulated gradually. Tuning the size of downsampling in pre-processing limits the number of points added to each voxel, thus balancing computational efficiency and accuracy. As long as the directions of \mathbf{n}_r (introduced in VII-A) and \mathbf{n}_d converge, we consider that the distribution stabilizes and fix it.

VII. SYSTEM DESCRIPTION

A. Data Pre-processing

To profile the environment with accurate local geometric information, instead of performing feature extraction on the raw points as in LOAM, LOG-LIO directly use Ring FALS (see V for details) to estimate the normal of each point, denoted as \mathbf{n}_r . Subsequently, voxel grid downsampling and backward propagation based on IMU measurements are used for point reduction and distortion correction, respectively.

B. Data Association

The IMU measurements are integrated from the previous frame as a prediction of the pose $\hat{\mathbf{x}}_k$ at the beginning of data association. With the prediction, each new coming LiDAR point ${}^{\mathcal{L}}\mathbf{p}_i$ transforms the world frame ${}^{\mathcal{W}}\mathbf{p}_i = {}^{\mathcal{W}}\hat{\mathbf{T}}_T^{\mathcal{L}} \mathbf{T}_{\mathcal{L}}^{\mathcal{L}} \mathbf{p}_i$.

Having normal and distribution of map points, LOG-LIO perform high-quality data association as follows:

1) *Visibility and Consistency Checks*: Map points are not visible to the LiDAR if the angle between the normal of the map point and the ray (vector from the query point to the LiDAR) is greater than 90 degrees. This false association usually occurs indoors, where the two planes of an object (e.g., a wall) are close to each other, which is called the double-side issue [20]. This incorrect association is eliminated directly.

The average angle between the normal of the query point and the normals of the associated map points indicates consistency. If the average angle is larger than α ($\alpha = 60^\circ$ in this paper), we consider it an inconsistent association and discard it.

2) *Hierarchical Association*: For query points satisfy visibility and consistency checks, a robust and accurate hierarchical association with point-to-surfel priority over point-to-plane and large-scale over small-scale is performed.

Modeled by distributions, the surfel represents more accurate local geometric information than coordinates. Large-scale surfel can be approximated by merging multiple small-scale distributions (see III-D for details) and is insensitive to noise thus providing more robust constraints than small-scale surfel. The point-to-surfel distance implies the quality of the constraint. For constraints with low-quality large-scale surfel, we associate the query point with the surfel of the voxel where the point is located, which must already be fixed.

If the quality of all surfel is poor, LOG-LIO follows LOAM for point-to-plane association.

C. Pose optimization

We adopt the iterated Kalman filter from FAST-LIO2 to optimize the pose. The prediction step of the Kalman filter implemented by integrating the IMU measurements from the last optimized state $\bar{\mathbf{x}}_{k-1}$ with the covariance matrix $\bar{\mathbf{P}}_{k-1}$.

For a point ${}^{\mathcal{W}}\mathbf{p}_i$ is already transformed to the world frame, the residual z_i is computed as:

$$\mathbf{z}_i = \mathbf{n}_j ({}^{\mathcal{W}}\mathbf{p}_i - {}^{\mathcal{W}}\mathbf{q}_j) \quad (12)$$

where \mathbf{n}_j is the normalized normal of the associated surfel or plane of \mathbf{p}_i , and ${}^{\mathcal{W}}\mathbf{q}_j$ is the point lying on the corresponding element.

Denote $\hat{\mathbf{x}}_k$ and $\hat{\mathbf{P}}_k$ with propagated state and covariance respectively, and they represent the prior Gaussian distribution for the state. Incorporate the prior distribution with all point-to-surfel and point-to-plane measurement models from (12) yields the maximum a-posterior estimate(MAP):

$$\begin{aligned} \min_{\tilde{\mathbf{x}}_k} & (\|\mathbf{x}_k - \hat{\mathbf{x}}_k\|_{\hat{\mathbf{P}}_k}^2 \\ & + \sum_{i \in \text{surfel}} \|\mathbf{z}_i^\kappa + \mathbf{H}_i^\kappa \tilde{\mathbf{x}}_k\|_{\mathbf{R}_i}^2 \\ & + \sum_{j \in \text{plane}} \|\mathbf{z}_j^\kappa + \mathbf{H}_j^\kappa \tilde{\mathbf{x}}_k\|_{\mathbf{Q}_j}^2) \end{aligned} \quad (13)$$

where $\tilde{\mathbf{x}}_k^\kappa$ is the error of the κ -th iterate update at time k , \mathbf{H}_i^κ and \mathbf{H}_j^κ are Jacobian matrices with respect to $\tilde{\mathbf{x}}_k^\kappa$, \mathbf{R}_i and \mathbf{Q}_j come from the raw measurement noise. The Kalman gain can be computed in an efficient way that the computation load depends on the state dimension instead of the measurement dimension. Due to limited space, we refer readers to [15], [16] for details.

D. Map Management

LOG-LIO manages maps with voxels. However recalculating the voxel point distribution when adding new points is overburdening for the LIO system. To incrementally maintain the points distribution within each voxel, we extend the ikdtree and mapping each voxel to a corresponding node.

VIII. EXPERIMENTAL RESULTS

A. Implementation

For the Ring FALS normal estimator, the lookup table is pre-built following $\mathcal{V}(\text{ring}_i, \text{column}_i) = \bar{\mathbf{v}}_i$, where $\text{row}_i = \text{ring}(\mathbf{p}_i)$, $\text{column}_i = \theta_i / \text{res}$ and res is the preset horizontal angle resolution. For each node of the extended ikdtree, we incrementally maintain the points distribution after the number of points in the voxel has accumulated to a certain number η ($\eta = 25$ in this paper). To balance efficiency and accuracy, we fix the distribution of voxels after the inside points reach 2η . The downsampling grid in data pre-processing is set to have the same size as the map to ensure that at most one point falls within a voxel for each frame. As long as the angle between the direction of \mathbf{n}_r and \mathbf{n}_d is less than 20 degree, the distribution is considered to be stabilized and the normals of the voxels are fixed as the average of \mathbf{n}_r and \mathbf{n}_d .

B. Experimental Design

The experiment focuses on the following two key points:

- Ring FALS estimates the normal of LiDAR points in real-time and accurately represents environmental information.
- By incorporating normal and points distribution estimation to accurately represent local geometric information, LOG-LIO improves the accuracy of pose estimation.

We conduct extensive experiments on the public datasets M2DGR [21] and NTU VIRAL [22] to prove the above two points. Experiments were carried out on a PC with Ubuntu 18.04, equipped with an Intel Core Xeon(R) Gold 6248R 3.00GHz processor and 32G RAM.

C. Ring FALS Normal Estimation

We compare Ring FALS and PCL [12] normal estimation tools. The implementation of PCL normal estimation is based on traditional least squares with the assistance of KDtree. By approximating the problem as estimating the normal to a plane tangent to the surface where the point is located, it becomes a least-squares plane fitting estimation problem. PCL also provides an additional implementation to speed up the computation, which uses the multi-threaded paradigm of OpenMP [23]. Considering that normal smoothing of disordered point cloud is another time-consuming process, the results of PCL are not further modified, but only smooth the normals of Ring FALS.

We visualize the normalized normals at the starting position of the sequence *gate03* of the M2DGR dataset to provide a intuitive evaluation. As shown in Fig. 3, almost all ground point normals are vertically upward. For the pillar shown in the yellow box in Fig. 3, from the top view, the normal at each point is perpendicular to the wall and the normal at the corner is smoothly articulated with the two adjacent sides. For more visualization results of normal estimation, we recommend readers go to <https://github.com/tiev-tongji/RingFalsNormal>.

Table I shows the average normal estimation processing times for a single scan of LiDAR used in the M2DGR and NTU VIRAL datasets, respectively. For a single scan of about 57,600 points for the Velodyne-32 LiDAR, Ring FALS takes a tenth of the time spent on PCL, and a quarter of it even compared to the OMP version. For the Ouster-16 LiDAR, the time consumption of Ring FALS is much less than that of PCL, no matter for the single threaded or OMP version. Analyzing the results of PCL, although Ouster-16 LiDAR has fewer points than Velodyne-32, the consumption time increases instead. The reason is that one of the most time-consuming parts of the PCL normal estimation is the KDtree neighborhood searching, which is related to the structure of the KDtree. And the structure of the constructed KDtree depends on the complexity of the environment, hence simply reducing the number of points cannot guarantee the speedup of the normal estimation in PCL. This means treating the point cloud as disordered, the sparsity of the point cloud could become a computational burden for the

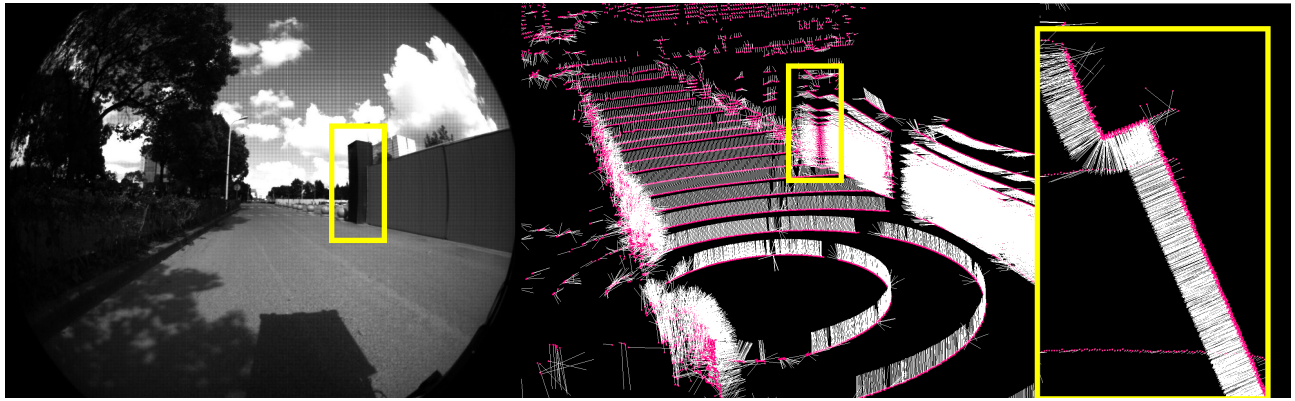


Fig. 3. The starting position of the sequence *gate03* of M2DGR dataset. The white lines represent normalized normals from Ring FALS estimation.

normal estimation. Although multi-threading speeds up the computation, how to choose a reasonable number of threads is also a problem to be considered. Ring FALS circumvents these problems because the structural information of the LiDAR is implicitly included in the lookup table.

D. Odometry Accuracy Evaluation

We compare LOG-LIO with two state-of-the-art LiDAR-Inertial SLAM methods, LIO-SAM [1] and FAST-LIO2 [16]. LOG-LIO and FAST-LIO2 estimate odometry without loop closure, for a fair comparison we disable the loop closure of LIO-SAM. Source code for LIO-SAM and FAST-LIO2 are obtained from the addresses they provide, and parameters remain as defaults. The root-mean-square error (RMSE) of the absolute trajectory error (ATE) is adopted to assess the accuracy of poses.

1) *M2DGR Datasets*: The dataset is collected by a ground robot and captured in diverse scenarios including both indoor and outdoor environments. The ground truth trajectories were obtained by a laser 3D tracker, motion capture device and an RTK receiver. In all experiments, the resolution of maps and new scan downsampling size was set to 0.4 m to reduce the interference of the point cloud density. Due to the instability of the RTK signal, the first 100 seconds and the last 100 seconds of *street07* and *street10* are discarded in the experiment, respectively. We evaluate the method combining the proposed Ring FALS, visibility and consistency checks (denoted as LOG-C) as ablation experiments.

Table II reports the result of our experiments. It can be seen that the trajectory accuracy of LOG, LOG-C and FAST-LIO2 is close in indoor scenes and outperforms LIO-SAM in most sequences. This makes sense because the number of plane features has a quantitative advantage in indoor scenes, where neighborhood map points generally form true planes. Therefore, the point-to-plane data association provides good constraints for pose estimation. Conversely, as errors accumulate, the point-to-line data association of LIO-SAM may provide negative effects. For outdoors, map points are relatively sparse compared to indoors, especially for the *street* sequences, where the robot moves on empty urban roads at night. Fig. 4 shows the trajectories of the sequence

street10 for qualitative comparison. The outstanding performance of LOG proves that surfel associated with map voxels better represents local geometric information in scenes with sparse points. However, the point-to-line and point-to-plane data associations become unstable as can be seen from the performance of LIO-SAM. Overall, with the visibility and consistency checks, LOG-C slightly improves the average accuracy. Combined with our proposed hierarchical data association and map management schemas, LOG performs the best, achieving the minimum error in 13 of the 21 sequences presented.

2) *NTU VIRAL Datasets*: NTU VIRAL performs data collection on an Unmanned Aerial Vehicle (UAV) platform with ground truth obtained by a laser-tracker total station with centimeter-level accuracy. The horizontal Ouster 16-channel OS1 LiDAR and VectorNav VN100 IMU are used for the experiments in this paper. Compared with M2DGR, the LiDAR used by VIRAL has a sparser point cloud, making it more challenging to estimate poses in open areas. In all experiments, the resolution of maps and new scan downsampling size is set to 0.5 m.

As shown in Table III, LOG-LIO gives the best results in most experiments, followed closely by FAST-LIO2, while LIO-SAM fails more often due to the sparsity of LiDAR point cloud and map. As the sequences *nya* and *tnp* traverse in small indoor areas, the errors of LOG-LIO and FAST-LIO2 are close, which is similar to M2DGR. For the sequences *eee*, *sbs* and *rtp*, although they are outdoor scenes, the drone is surrounded by buildings like indoors. The trajectories of LOG-LIO and FAST-LIO2 are also very close because of the well constrained plane. However, in the *spms* sequences, the UAV takes off from an area surrounded by buildings and then hovers at an altitude higher than the top of the surrounding buildings. The sparse point cloud obtained by the horizontal LiDAR has a low overlap with the map, therefore the registration error based on point-to-plane data association is prone to be large. For LOG-LIO, the points are first associated with the voxels where they are located, and the results show that the proposed hierarchical association tend to be higher-quality constrain.

TABLE I
THE MEAN RUNNING TIME(MS) OF NORMAL ESTIMATION FOR A SINGLE SCAN TO CERTAIN LiDARS

	points	projection	Ring FALS			total	PCL	
			box-filtering	smoothing	single thread		OMP 10 threads	
Velodyne-32	57600	2.045	2.540	3.199	7.784	79.811	26.355	
Ouster-16	16384	0.560	1.221	0.815	2.597	155.972	39.664	

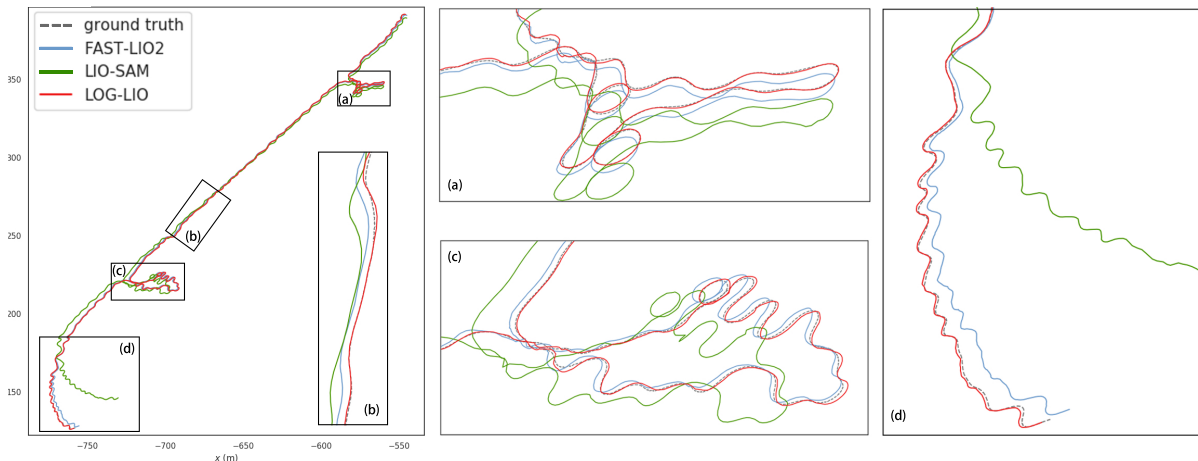


Fig. 4. Localization estimates in sequence *street10* of the M2DGR dataset. The zoomed in image of the colored boxes corresponds to the boxes of the same color in the trajectory.

TABLE II
THE TRANSLATION RMSE(M) RESULTS OF POSE ESTIMATION
COMPARISON ON THE M2DGR DATASET

Seq	duration (s)	LOG	LOG-C	LIO-SAM	FAST-LIO2
gate01	172	0.137	0.133	0.170	0.134
gate02	327	0.290	0.304	0.318	0.304
gate03	283	0.108	0.108	0.110	0.110
walk01	291	0.079	0.082	0.078	0.091
door01	461	0.250	0.250	0.271	0.253
door02	127	0.178	0.178	0.185	0.178
street01	1028	0.212	0.212	0.586	0.221
street02	1227	2.537	2.315	3.619	2.394
street03	354	0.140	0.146	0.149	0.140
street04	858	0.525	0.591	1.022	0.568
street05	469	0.342	0.310	0.491	0.319
street06	494	0.392	0.437	0.373	0.439
street07	829	2.301	3.468	1.514	3.422
street08	491	0.169	0.179	0.212	0.182
street09	907	3.010	3.570	2.447	3.613
street10	810	0.329	1.213	8.097	1.256
hall01	351	0.256	0.257	0.287	0.257
hall02	128	0.275	0.275	0.290	0.279
hall03	164	0.340	0.343	0.612	0.346
hall04	181	0.943	0.943	1.078	0.945
hall05	402	1.047	1.046	1.010	1.046
mean		0.660	0.779	1.091	0.786

3) *Processing Time Evaluation*: We statistics the average time consumption of LOG-LIO and FAST-LIO2 in every sequence as shown in table IV. Since the distribution of points within the map voxels is maintained incrementally, the average processing time on each scan in LOG-LIO is slightly longer than in FAST-LIO2. According to the number

TABLE III
THE TRANSLATION RMSE(M) RESULTS OF POSE ESTIMATION
COMPARISON ON THE NTU VIRAL DATASET

Seq	duration (s)	LOG-LIO	FAST-LIO2	LIO-SAM
eee_01	399	0.191	0.193	0.206
eee_02	321	0.141	0.142	0.145
eee_03	181	0.186	0.185	0.206
nya_01	396	0.208	0.204	0.278
nya_02	428	0.212	0.211	0.204
nya_03	411	0.224	0.224	0.305
sbs_01	354	0.222	0.222	x
sbs_02	373	0.208	0.208	0.211
sbs_03	389	0.195	0.194	0.203
rtp_01	482	0.206	0.236	x
rtp_02	453	0.201	0.201	0.182
rtp_03	355	0.195	0.196	0.158
tnp_01	583	0.174	0.171	x
tnp_02	457	0.167	0.167	x
tnp_03	407	0.206	0.202	x
spms_01	446	1.939	1.935	0.600
spms_02	398	2.401	3.388	x
spms_03	386	0.684	0.760	x
mean		0.442	0.502	x

of points and the complexity of the environment, LOG-LIO takes about 5 milliseconds more on average, but still meets the real-time requirements.

IX. CONCLUSION AND FUTURE WORK

This paper proposes LOG-LIO, an online LiDAR-inertial odometry, which incorporates real-time estimation of normal and points distribution to accurately represent the local

TABLE IV
THE AVERAGE TIME CONSUMPTION(MS) OF EACH SEQUENCE IN THE EXPERIMENTS

	M2DGR					NTU VIRAL						mean
	gate	walk	door	street	hall	eee	nya	sbs	rtp	tnp	spms	
LOG-LIO	39.839	40.382	18.073	36.380	18.603	18.806	15.421	15.724	23.530	17.122	20.948	25.321
FAST-LIO2	31.378	32.276	14.754	28.970	15.509	15.705	12.476	12.785	21.006	13.340	17.106	20.523

geometric information. An efficient normal estimator for LiDAR point cloud, namely Ring FALS, is also presented, which pre-computes the bearing information and uses only the range information to estimate the normal of points. LOG-LIO manages the map with an extended ikd-tree and incrementally maintains the normal and points distribution within the map voxels. The hierarchical data association schema provides accurate constraints resulting in more accurate pose estimation. LOG-LIO outperforms state-of-the-art LIO systems in our experiments on diverse environments.

For future work, we plan to incorporate dynamic noise removal and loop closure in LOG-LIO to improve stability in dynamic environments and long-term operation.

REFERENCES

- [1] T. Shan, B. Englot, D. Meyers, W. Wang, C. Ratti, and D. Rus, "Lio-sam: Tightly-coupled lidar inertial odometry via smoothing and mapping," in *2020 IEEE/RSJ international conference on intelligent robots and systems (IROS)*. IEEE, 2020, pp. 5135–5142.
- [2] H. Ye, Y. Chen, and M. Liu, "Tightly coupled 3d lidar inertial odometry and mapping," in *2019 International Conference on Robotics and Automation (ICRA)*. IEEE, 2019, pp. 3144–3150.
- [3] C. Qin, H. Ye, C. E. Pranata, J. Han, S. Zhang, and M. Liu, "Lins: A lidar-inertial state estimator for robust and efficient navigation," in *2020 IEEE international conference on robotics and automation (ICRA)*. IEEE, 2020, pp. 8899–8906.
- [4] A. Reinke, M. Palieri, B. Morrell, Y. Chang, K. Ebadi, L. Carlone, and A.-A. Agha-Mohammadi, "Locus 2.0: Robust and computationally efficient lidar odometry for real-time 3d mapping," *IEEE Robotics and Automation Letters*, vol. 7, no. 4, pp. 9043–9050, 2022.
- [5] K. Chen, B. T. Lopez, A.-a. Agha-mohammadi, and A. Mehta, "Direct lidar odometry: Fast localization with dense point clouds," *IEEE Robotics and Automation Letters*, vol. 7, no. 2, pp. 2000–2007, 2022.
- [6] T.-M. Nguyen, D. Duberg, P. Jensfelt, S. Yuan, and L. Xie, "Slic: Multi-input multi-scale surfel-based lidar-inertial continuous-time odometry and mapping," *IEEE Robotics and Automation Letters*, vol. 8, no. 4, pp. 2102–2109, 2023.
- [7] M. Palieri, B. Morrell, A. Thakur, K. Ebadi, J. Nash, A. Chatterjee, C. Kanellakis, L. Carlone, C. Guaragnella, and A.-a. Agha-Mohammadi, "Locus: A multi-sensor lidar-centric solution for high-precision odometry and 3d mapping in real-time," *IEEE Robotics and Automation Letters*, vol. 6, no. 2, pp. 421–428, 2020.
- [8] M. Ramezani, K. Khosoussi, G. Catt, P. Moghadam, J. Williams, P. Borges, F. Pauling, and N. Kottege, "Wildcat: Online continuous-time 3d lidar-inertial slam," *arXiv preprint arXiv:2205.12595*, 2022.
- [9] J. Zhang and S. Singh, "Loam: Lidar odometry and mapping in real-time," in *Robotics: Science and Systems*, vol. 2, no. 9. Berkeley, CA, 2014, pp. 1–9.
- [10] H. Badino, D. Huber, Y. Park, and T. Kanade, "Fast and accurate computation of surface normals from range images," in *2011 IEEE International Conference on Robotics and Automation*. IEEE, 2011, pp. 3084–3091.
- [11] R. Fan, H. Wang, B. Xue, H. Huang, Y. Wang, M. Liu, and I. Pitas, "Three-filters-to-normal: An accurate and ultrafast surface normal estimator," *IEEE Robotics and Automation Letters*, vol. 6, no. 3, pp. 5405–5412, 2021.
- [12] R. B. Rusu and S. Cousins, "3d is here: Point cloud library (pcl)," in *2011 IEEE international conference on robotics and automation*. IEEE, 2011, pp. 1–4.
- [13] A. Segal, D. Haehnel, and S. Thrun, "Generalized-icp," in *Robotics: science and systems*, vol. 2, no. 4. Seattle, WA, 2009, p. 435.
- [14] M. Kaess, H. Johannsson, R. Roberts, V. Ila, J. J. Leonard, and F. Dellaert, "isam2: Incremental smoothing and mapping using the bayes tree," *The International Journal of Robotics Research*, vol. 31, no. 2, pp. 216–235, 2012.
- [15] W. Xu and F. Zhang, "Fast-lio: A fast, robust lidar-inertial odometry package by tightly-coupled iterated kalman filter," *IEEE Robotics and Automation Letters*, vol. 6, no. 2, pp. 3317–3324, 2021.
- [16] W. Xu, Y. Cai, D. He, J. Lin, and F. Zhang, "Fast-lio2: Fast direct lidar-inertial odometry," *IEEE Transactions on Robotics*, vol. 38, no. 4, pp. 2053–2073, 2022.
- [17] C. Yuan, X. Liu, X. Hong, and F. Zhang, "Pixel-level extrinsic self calibration of high resolution lidar and camera in targetless environments," *IEEE Robotics and Automation Letters*, vol. 6, no. 4, pp. 7517–7524, 2021.
- [18] C. Yuan, W. Xu, X. Liu, X. Hong, and F. Zhang, "Efficient and probabilistic adaptive voxel mapping for accurate online lidar odometry," *IEEE Robotics and Automation Letters*, vol. 7, no. 3, pp. 8518–8525, 2022.
- [19] M. McDonnell, "Box-filtering techniques," *Computer graphics and image processing*, vol. 17, no. 1, pp. 65–70, 1981.
- [20] L. Zhou, D. Koppel, and M. Kaess, "Lidar slam with plane adjustment for indoor environment," *IEEE Robotics and Automation Letters*, vol. 6, no. 4, pp. 7073–7080, 2021.
- [21] J. Yin, A. Li, T. Li, W. Yu, and D. Zou, "M2dgr: A multi-sensor and multi-scenario slam dataset for ground robots," *IEEE Robotics and Automation Letters*, vol. 7, no. 2, pp. 2266–2273, 2021.
- [22] T.-M. Nguyen, S. Yuan, M. Cao, Y. Lyu, T. H. Nguyen, and L. Xie, "Ntu viral: A visual-inertial-ranging-lidar dataset, from an aerial vehicle viewpoint," *The International Journal of Robotics Research*, vol. 41, no. 3, pp. 270–280, 2022.
- [23] R. Chandra, L. Dagum, D. Kohr, R. Menon, D. Maydan, and J. McDonald, *Parallel programming in OpenMP*. Morgan kaufmann, 2001.